

LiNO₃-Free CNT Li-S Batteries towards Safe, High Specific Energy Storage:
Mechanistic Studies, Ratio Effects, CNT Parameters,
and Other Practical Considerations

Sterling Gregory Baird

A senior thesis submitted to the faculty of
Brigham Young University
in partial fulfillment of the requirements for the degree of

Bachelor of Science

Robert Davis, Advisor

Department of Physics and Astronomy
Brigham Young University
September 2018

Copyright © 2018 Sterling Baird
All Rights Reserved

ABSTRACT

LiNO₃-Free CNT Li-S Batteries towards Safe, High Specific Energy Storage:
Mechanistic Studies, Ratio Effects, CNT Parameters,
and Other Practical Considerations

Sterling Baird
Department of Physics and Astronomy, BYU
Bachelor of Science

The high theoretical gravimetric energy density (Wh/kg) of lithium-sulfur batteries holds promise for battery applications such as UAVs, electric vehicles, and military applications. Here, we report the use of a carbon nanotube based interfacial layer in conjunction with highly scalable sulfur cathodes using the doctor-blade coating technique for high capacity, highly coulombic efficient lithium-sulfur batteries. The interfacial layer consists of vertically-aligned multi-walled carbon nanotubes and a conductive nonporous layer which aids in polysulfide trapping. We observe a high initial discharge capacity of 930 mAh/g-S and high coulombic efficiencies above 93% without the use of gas-forming additives such as lithium nitrate. Ratio effects between sulfur, electrolyte, and lithium reveal correlations to lower capacity with higher sulfur loading, higher capacity with stronger electrolyte to sulfur ratios, and increased cycle life with greater lithium overcapacity. Overcharge experiments reveal that a 15% overcharge cut-off provides reasonable efficiency (~87%), and cycle life. Addition of 1% selenium to the cathode composition increased discharge voltages, but slightly decreased capacity and did not have a discernable effect on rate capability at 1C. Addition of PEO/LiTFSI/HNT binder stabilized cycling, but decreased capacity in some instances. Enhanced diffusion pathways and electrolytic contact had a positive correlation with capacity, suggesting that micro-patterned carbon nanotube architectures may play a unique role in lithium-sulfur batteries.

ACKNOWLEDGEMENTS

Thank you to Dr. Robert Davis for serving as my mentor and facilitating funding for this research opportunity over the course of several years and to Lawrence Barrett for training me on the basics of carbon nanotube micro-fabrication and battery research. Thank you also to Dr. Richard Vanfleet, Dr. John Harb, Kevin Laughlin, and Rita Fan for useful guidance. Of course, I would also like to acknowledge my family and my wife, Victoria Baird, for unrelenting support and motivation.

1	Table of Contents	
1	Chapter 1: Introduction	6
2	Chapter 2: Experimental Methods	9
2.1	Fabrication of sulfur cathode	9
2.2	Fabrication of encapsulated interfacial layer	10
2.3	Fabrication of electrolyte	11
2.4	Fabrication of thin lithium anodes	12
2.5	Other methods	12
3	Chapter 3: Results and Discussion	13
3.1	Comparison with other Li-NO ₃ free studies	13
3.2	Post-cycling SEM and EDS	14
3.3	Ratio Effects	16
3.3.1	Effect of EL:S ratios, electrolyte loading, and sulfur loading	16
3.3.2	Effect of lithium overcapacity	17
3.4	Cycling Conditions	19
3.4.1	Effect of overcharge end condition	19
3.5	Slurry Cathode Modifications	20
3.5.1	Addition of 1% Se Additive	21
3.5.2	Addition of PEO/LiTFSI Binder	22
3.6	Decoupling diffusion and conductivity	23
4	Chapter 4: Conclusions and Future Outlook	26
4.1	Conclusions	26
4.2	Ideas for enhancing performance	28
5	Appendix A – Supplementary Experiments	29
5.1	Supplemental Experiment 1	29
5.2	Supplemental Experiment 2	30
6	Appendix B – Challenges of the Lithium-Sulfur Chemistry	31
6.1	Physical challenges of the lithium-sulfur chemistry	31
6.1.1	Conductivity of sulfur	31
6.1.2	Volume expansion of sulfur	31
6.1.3	Dissolution of polysulfides	31
6.1.4	Lithium dendrites	32

6.1.5	Parasitic reactions of polysulfides with electrolyte/anode.....	32
6.1.6	Polysulfide shuttle mechanism	32
6.2	Practical challenges of commercializing lithium-sulfur batteries	32
6.2.1	Cathode mass fraction.....	32
6.2.2	Sulfur loading.....	33
6.2.3	Electrolyte to Sulfur Ratios.....	33
6.2.4	Lithium overcapacity	34
6.2.5	Low coulombic efficiency/infinite-charge syndrome.....	34
6.2.6	Low cycle life	35
7	Appendix C – Chain reaction effects.....	35
7.1	CNT Parameters	37
7.1.1	Un-patterned, encapsulated CNTs	37
7.1.2	Presence of floor layer in encapsulated cells	37
8	Appendix D – Supplementary Experimental Methods.....	39
8.1	SEM and EDS characterization of samples.....	39
8.1.1	Calendaring.....	40
8.2	Roll Press Modifications (2018-06w1,2...pptx on box).....	40
8.2.1	Free-standing slurry electrodes via roll-press	40
8.2.2	Roll-press of CNTs and cathode slurry.....	41
8.3	Lithium anode modifications	42
8.3.1	Lithium melt infiltration into CNTs via LPCVD lithophilic coating	42
8.4	Bibliography	44
8.5	Index	47

1 Chapter 1: Introduction

The high energy per mass and the high energy affordability of sulfur make the lithium-sulfur (Li-S) chemistry appealing for applications such as renewable energy, military, UAV, and electric vehicle applications. Specific energy or gravimetric energy density refers to energy stored per unit mass, typically Wh/kg. Li-S has a high theoretical specific energy of ~2500 Wh/kg compared with other chemistries (Figure 1). Sulfur itself has a high theoretical specific capacity of 1675 mAh/g. Achieving the high theoretical specific energy of the lithium-sulfur chemistry requires low amounts of inactive or excess components such as the electrolyte and anode. On the cost side, bulk elemental sulfur is estimated to be ~\$100/ton. Traditional lithium-ion battery components (cobalt, nickel, iron, manganese) cost up to several orders of magnitude more. The low overall cost of lithium-sulfur batteries can only be realized if the prices of all components are considered and the energy per cost is favorable overall.

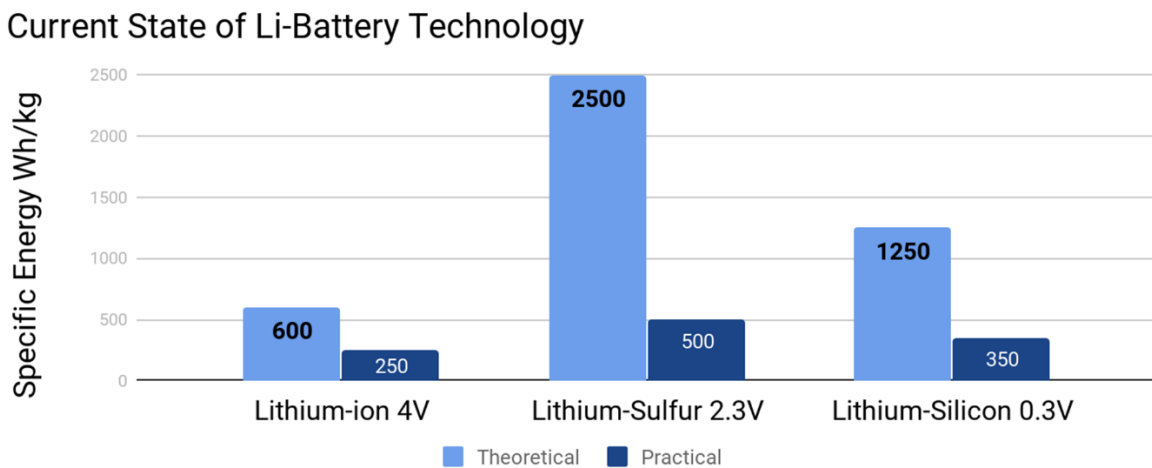


Figure 1. comparison of various Li-ion practical and theoretical specific capacities vs. next generation chemistries.

Many physical challenges, however, complicate the practical use of this promising chemistry (Figure 2). For example, sulfur is a poor conductor and expands by 80% when converted to Li_2S . Conductive additives such as carbon black and porous materials with room for volume expansion accommodate these issues. Additionally, intermediate sulfur compounds (e.g. Li_2S_6) dissolve in many organic electrolytes causing loss of active material from the cathode, parasitic reactions with the anode, and a unique “shuttle” mechanism causing low efficiencies. Like many other lithium-metal based chemistries, lithium dendrites can form. While addressing these physical challenges, one must also be able to address practical challenges such as increasing cathode active material fraction and minimizing the amount and cost of excess materials. For nearly all battery applications, a high level of safety is also required. More details concerning each of these physical challenges can be found in Appendix B – Challenges of the Lithium-Sulfur Chemistry.

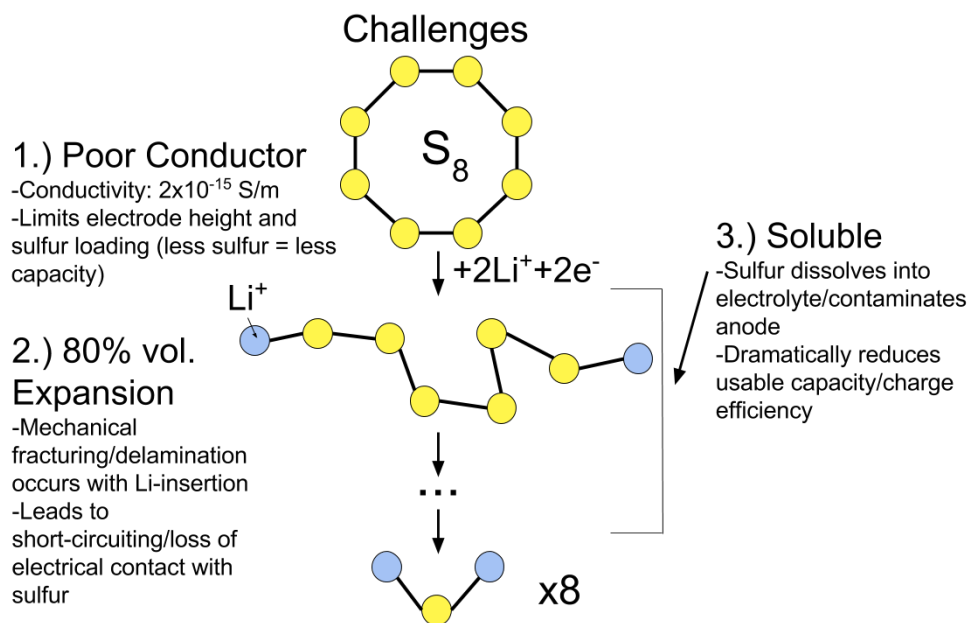


Figure 2. Diagram demonstrating key physical challenges of the lithium-sulfur chemistry: poor conductivity, volume expansion, and solubility issues.

Many have employed the use of binders, barriers, protective coatings, and other modifications to the cathode, anode, separator, and electrolyte to address these unfavorable issues. Unfortunately, a high percentage (~98%) of experimental lithium-sulfur battery articles employ an unsafe additive, lithium-nitrate (LiNO_3), commonly used in fireworks and other explosives. LiNO_3 is a strongly oxidizing compound that has been shown to create a stable solid-electrolyte-interphase (SEI) layer on the lithium anode, increasing coulombic efficiency and cycle life. LiNO_3 is continuously consumed during cycling, necessitating large initial concentrations. It is therefore unlikely to be successful in smaller quantities that could be considered safer. Such an additive in a high-energy cell containing flammable, toxic electrolytes and combustible lithium metal presents a compounded safety hazard in addition to increased cost. This calls for other methods to improve the practical performance of lithium-sulfur batteries while maintaining safety.

In this work, we seek to take a balanced approach addressing the various physical and practical challenges associated with a LiNO_3 -free Li-S chemistry. This study addresses the use of micro-patterned carbon nanotube (CNT) architectures as an interfacial layer (Figure 3) to enhance conductivity, allow for volume expansion, and retain polysulfides in the cathode without the use of LiNO_3 . Effects of key parameters such as sulfur loading, EL:S ratios, and lithium overcapacity are explored. Additionally, parameters such as overcharge cut-off and cathode modification are presented.

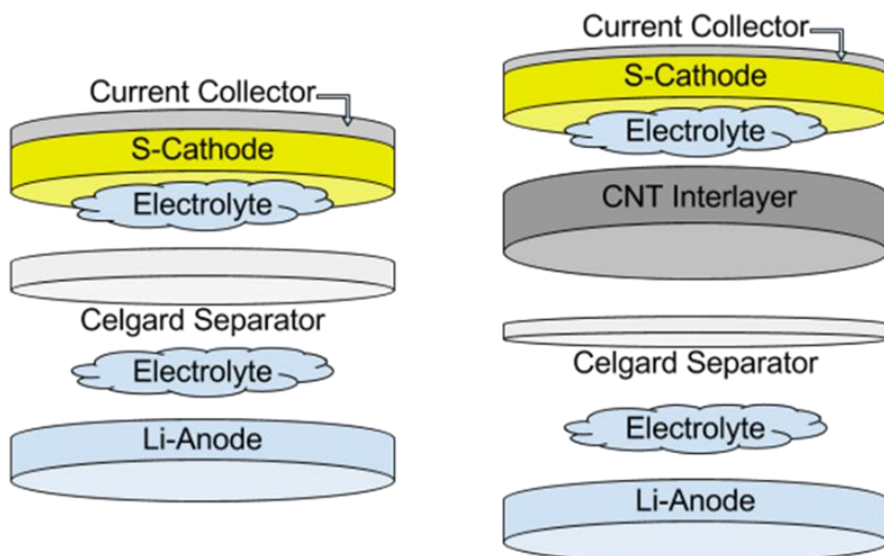


Figure 3. Schematic of a traditional lithium-sulfur cell with a slurry cathode and LiNO₃ additive in electrolyte (left). Schematic of as-assembled lithium-sulfur battery using a carbon nanotube design with a conductive nonporous coating and 70%-S, 20% Carbon Black, 10% PVdF (by wt.) sulfur cathode (right). The carbon nanotubes (~100 μm height) are a highly conductive scaffolding that facilitates electron transport and increases structural stability, synthesized via chemical vapor deposition using an Fe-catalyst and C₂H₄ precursor. A conductive, nonporous coating is added to prevent sulfur dissolution for higher sulfur retention and protection of the Li-anode.

2 Chapter 2: Experimental Methods

2.1 Fabrication of sulfur cathode

Approximately 0.15 g Polyvidiline fluoride (PVdF) binder (company) was placed in 7.5 mL 1-Methyl-2-pyrrolidone (NMP) and heated in a sealed container via boiling water bath for ~2 hours to facilitate dissolution of the binder. Following dissolution, ~1.05 g elemental Sulfur powder (company) and ~0.3 g Carbon Black (Sigma Aldrich) was placed in the solution and

homogenized via ultra-sonic probe for ~15 minutes to form a S/CB/PVdF (70%/20%/10% by wt.) slurry. The slurry was then spread onto Al-foil (~7 microns thick) using the doctor-blade technique. The Al-foil was cleaned with a slight amount of NMP on a towelette prior to coating. The slurry-coated Al-foil was then placed in an oven at ~60°C for several hours to dry. Disks (14.5 mm in diameter) were then punched. A 1.125 cm² cylinder was placed at the center of the cathode and excess slurry was scraped off with a razor blade. The exposed Al-foil was then crimped around the edges of a 1 cm² interfacial layer for the as-assembled cathode and interfacial layer combination with 1.125 cm² as the final diameter. Areal loading was determined to be ~3 mg-S/cm². The interfacial layer used was approximately 100 microns tall. Total mass of the cathode and interfacial layer was determined to be 6.11 mg (not including current collector).

2.2 Fabrication of encapsulated interfacial layer

A Si/Al₂O₃ substrate is patterned using photolithography on AZ3330 photoresist in class 10 cleanroom. A thin film of iron (4nm) is deposited by thermal evaporation. Photoresist is then removed via sonication in NMP, including iron-coated photoresist. VA-MWCNTs are grown via chemical vapor deposition (CVD) @ 750°C with H₂ and C₂H₄ on Al₂O₃ (e-beam evaporated)/Si- wafer using 4 nm Fe as catalyst. VA-MWCNTs are then infiltrated with carbon @ 900°C with the same catalyst gases. Typically, the sample is then saturated with silicon via low-pressure chemical vapor deposition (LPCVD) for 80 min @ 535°C and 300 mTorr. A carbon blanket-layer is deposited via CVD (H₂/C₂H₄) @ 900°C onto the Si-saturated CNT-forest for 10-60 min, also resulting in self-delamination of forest from wafer. Carbon floor layer of forest is etched via O₂ plasma to expose Si for removal via KOH (30% KOH by wt. in water, for 1 hour @ 70°C), resulting in a flexible, encapsulated interfacial layer (Figure 5).

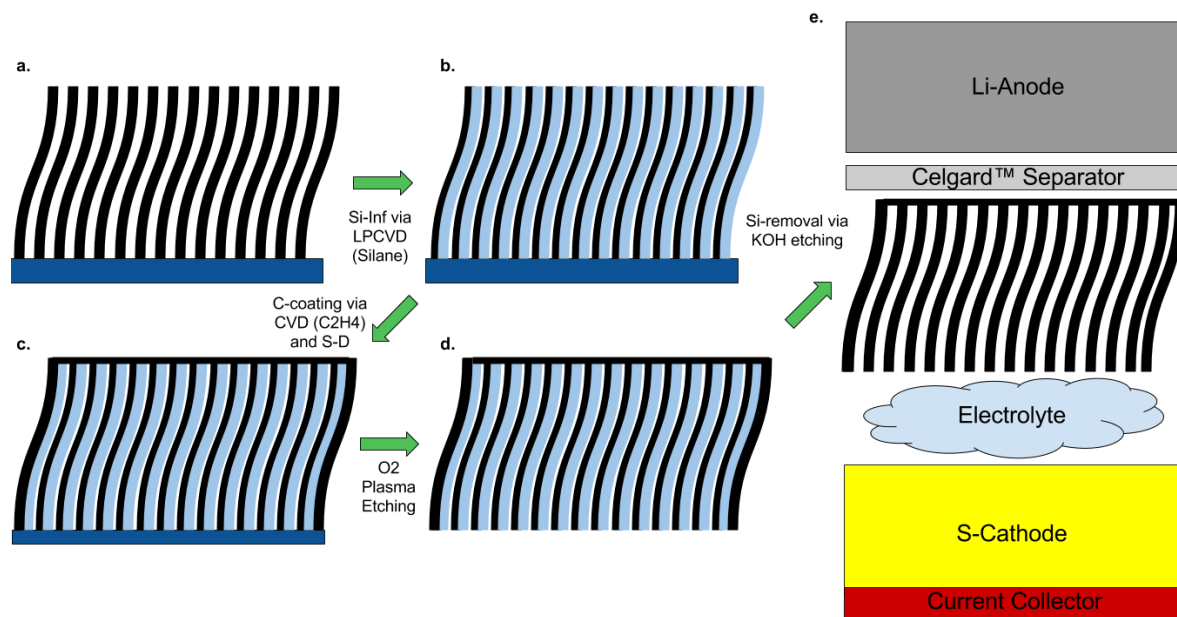


Figure 4. Fabrication of encapsulated interfacial layer. a. VA-MWCNTs grown on Si/Al₂O₃ substrate. b. VA-MWCNTs saturated with silicon via low-pressure chemical vapor deposition. c. Chemical vapor deposition carbon coating applied to Si-saturated forest using ethylene as precursor, resulting in self-delamination from substrate. d. substrate facing side etched with O₂ plasma. e. fully assembled cell using encapsulated VA-MWCNT interfacial layer with Si-removal via KOH etching.

2.3 Fabrication of electrolyte

Typically ~0.2 M Lithium Bis(trifluoromethane)sulfonide (Sigma-Aldrich 99.5% anhydrous(?)) in (1:1, v:v) 1,2 dimethyl ether (DME, Sigma Aldrich) and 1,3 dioxolane (DIOX, Sigma-Aldrich), mixed for 3 minutes by magnetic stirring at moderate intensity. Various electrolyte to sulfur (E/S) ratios were obtained. The electrolyte mass was measured by subtracting mass of all other components from the mass of the post-assembled cell with electrolyte.

2.4 Fabrication of thin lithium anodes

Due to the ductile nature of lithium, the metal covers a larger surface area when pressure is applied. A hydraulic press was implemented to spread a small amount of lithium (~2-5 mg) across a larger surface area, thus yielding thin lithium anodes. When lithium was pressed against another metal, it tended to stick to the surface and not come off without causing some defect to the lithium metal. An alternative strategy was implemented using Celgard. First, a lithium chip was scraped free of oxide layers using a stainless-steel scalpel. Second, a small square of the lithium was cut using the scalpel. Third, the piece was sandwiched between two pieces of Celgard separator material and pressed together using a hydraulic press. Last, one or both Celgard layers was peeled off using tweezers (Figure 26). Often, one Celgard layer could remain and function as the separator. However, when assembled, the battery tended to short-circuit likely due to cuts observable in the Celgard layer post-pressing. Therefore, a second separator was often added to prevent short-circuiting. These thinner anodes were used in the lithium overcapacity experiments.

2.5 Other methods

Cells were assembled according to schematic in Figure 3 using CR2025 coin cell configuration inside dry argon-environment (less than 1 ppm). Galvanostatic charge/discharge plots were obtained via MACCOR Battery Testing Equipment. Typical cells were charged and discharged at C/20 for one cycle, C/4 for the second cycle, and C/10 for the rest of the cycles in the voltage range of 1.8 - 2.6 V for a total of 103 cycles (1C = 1675 mAh/g). Cells were disassembled, and cathodes were rinsed in DME/DIOX (1:1/v:v) several times before imaging, unless otherwise noted. SEM images obtained via (S-Feg XL30 FEI) using EDS (EDAX) equipment and software.

3 Chapter 3: Results and Discussion

3.1 Comparison with other Li-NO₃ free studies

Li-S batteries employing micro-patterned CNT forests demonstrate reasonably competitive performance compared with other Li-NO₃ free studies. In one study by ..., the lithium anode was pre-treated in a soaking solution of LiNO₃ for three days prior to being assembled into a battery, achieving reasonable efficiency, capacity, and sulfur loading. This battery attained an average coulombic efficiency of 87.2% and 700 mAh/g over 100 cycles with 3.25 mg-S/cm². Our work attains similar metrics: above 90% efficiency and 600 mAh/g average over 100 cycles at 3.5 mg-S/cm² (Figure 5). Additionally, it is unknown to what extent the pre-treatment using LiNO₃ provides safety advantages over LiNO₃ as an additive. Unless alternative encapsulation methods are developed, however, a lengthy LiNO₃ pretreatment process may be the more economical route. Several alternative methods are discussed in 4.2.

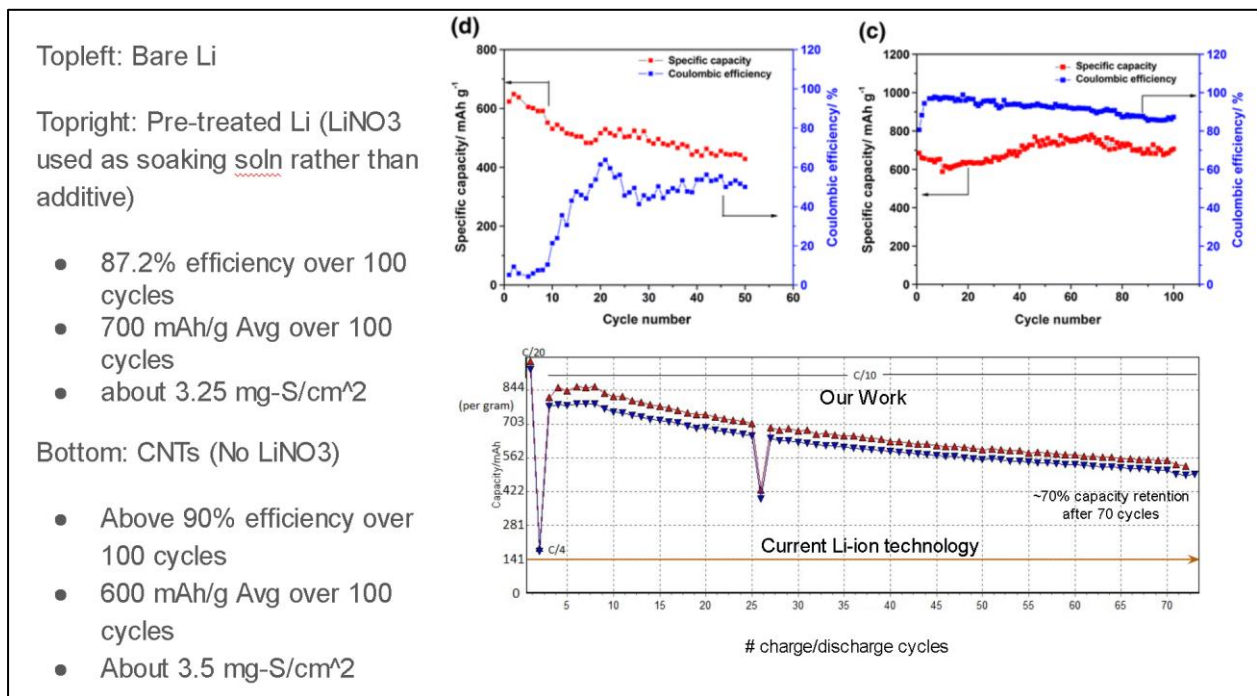


Figure 5. Comparison of our work (bottom-right) with another LiNO₃ free work (d, c).

Post-cycling results assert the effectiveness of the interfacial layer in trapping polysulfides at the cathode. The CNT encapsulation layer penetrates through each of the through-holes, contributing to a better restricted diffusion network (Figure 6). Additionally, SEM and EDS results reveal a high sulfur concentration within the CNT structure post-cycling (Figure 7).

3.2 Post-cycling SEM and EDS

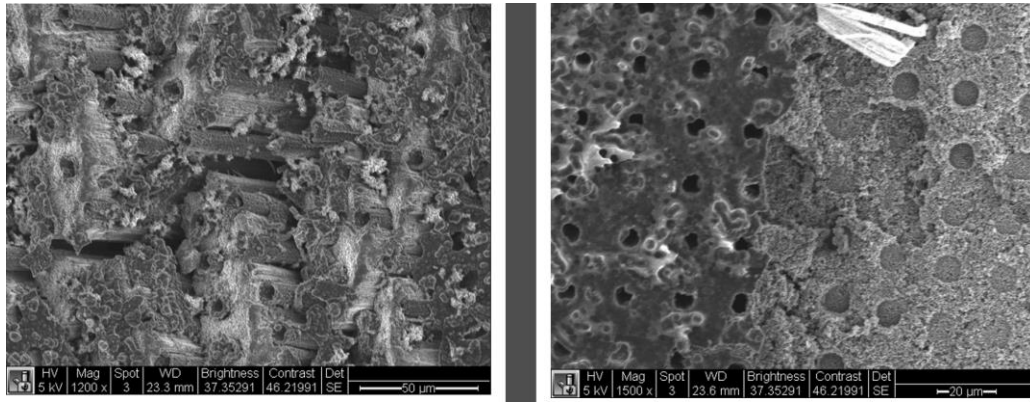


Figure 6. Top-view SEM images of CNTs after 100 cycles at 45° tilt (left) showing inside pillars and 0° tilt (right) showing boundary between microstructure and underlying slurry.

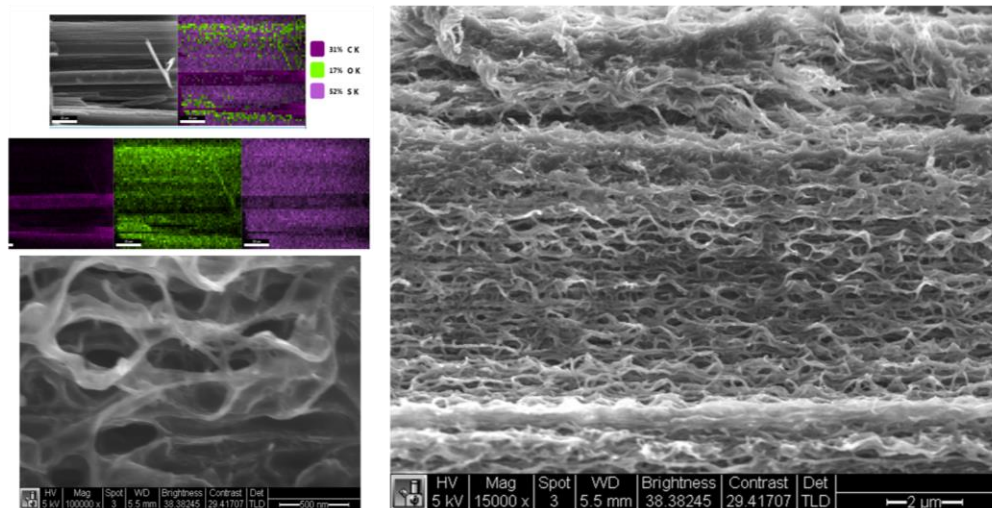


Figure 7. SEM images of S-coated CNTs after 100 cycles (bottom-left, right) and corresponding EDS data (top-left insets) demonstrating sulfur retention at the cathode side (lighter purple).

Rate capability did not seem to improve with the encapsulation layer. Rather, slurries without the interfacial layer had better rate performance. A later CNT-cathode with many fissures had favorable rate performance on the 2nd cycle, as well as from the 104th cycle on. An interfacial layer seems to reduce shuttle because of higher coulombic efficiency (STR_016 results -> 2.6 V cutoff, ~93% CE). Meanwhile, the broken, patterned encapsulation layer without a floor layer seemed to have better capacity retention compared with more intact ones (Figure 8).

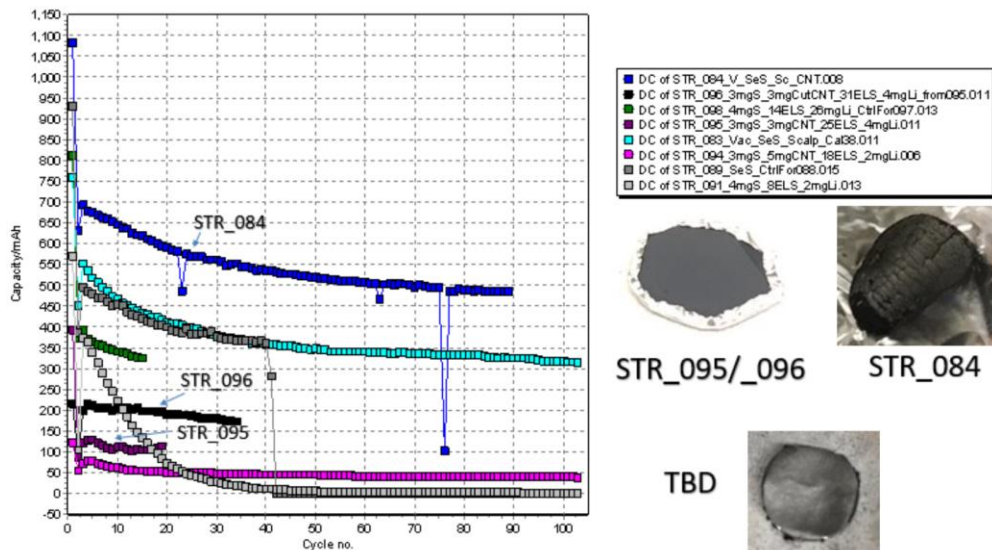
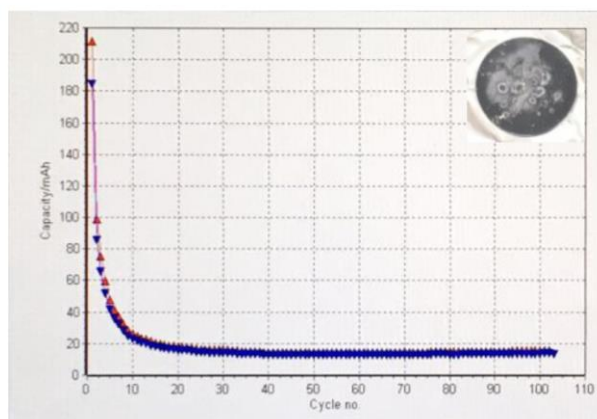


Figure 8. Cycling comparison of cracked CNTs versus intact CNTs.

Encapsulated cells with slurry have much better retention and utilization than unencapsulated CNT and no slurry counterparts. So far, the sacrificial etch cells seem to do much better than the floor layer encapsulations. While some results have been acquired for alternative trapping layers (Figure 9), this has not been tested extensively.

Name	Type	Growth/Inf	Height	CNT Mass	Se Mass	S Mass	Total Mass	Porosity
STR_081	Cathode	60min/2min	~600 um	3.46 mg	8.18 mg	16.73 mg	28.37	~72%



Low specific capacity: ~180 mAh/g

Initial discharge capacity: ~5 mAh

High C/20 current: 1.678 mA

Low EL/S Ratio: 3.08

115% Overcharge

Figure 9. Floor layer used as encapsulation layer in Se/S battery and stand-alone CNT structure. Selenium and sulfur were melt-infiltrated into the CNTs. Tops of the CNTs were made to contact the stainless-steel cap of the battery.

3.3 Ratio Effects

3.3.1 Effect of EL:S ratios, electrolyte loading, and sulfur loading

Lithium-sulfur batteries tend to require much higher electrolyte to active mass ratios (e.g. > 5:1) than traditional lithium-ion batteries (~1:1). When electrolyte to sulfur (EL:S) ratios are too low (e.g. < 5:1), increased electrolyte viscosity will dramatically increase cell resistance and thereby lower sulfur utilization in many Li-S configurations (1). When EL:S ratios are exorbitantly high (e.g. > 15:1), the advantage of high theoretical specific energy is forfeited. Additionally, because this metric affects performance through electrolyte viscosity and cell impedance, the performance of electrolyte-flooded coin cells will not necessarily correlate with the performance of electrolyte-lean pouch cells.

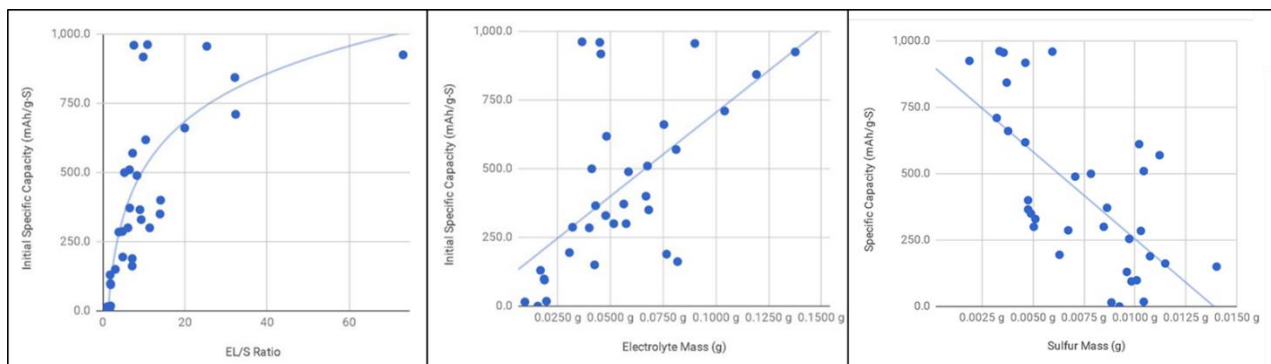


Figure 10. EL:S ratios for many different batteries show a general trend that higher EL:S ratio as well as higher electrolyte mass corresponds to higher capacity (left). More electrolyte and higher sulfur loading generally corresponds with high and low specific capacity, respectively.

High sulfur loading can increase energy affordability and specific energy by increasing the fraction of sulfur compared with other inactive components such as current collectors, separators, and battery housing. As sulfur load increases, electronic and ionic resistance can begin to dominate as transport lengths increase and reaction sites are shielded. This leads to reduced sulfur utilization, suggesting an optimal sulfur load for best performance.

3.3.2 Effect of lithium overcapacity

Lithium overcapacity refers to the excess stoichiometric amount of lithium compared with the sulfur active material present in the battery. A lithium overcapacity of 0% means that for complete conversion of all elemental sulfur and lithium into lithium-sulfide, all reactants will be used up. It is recognized that some excess amount of lithium is necessary for the proper functioning of lithium-sulfur and other lithium-metal chemistries (2-4). In many studies, lithium overcapacity exceeds 3000%, resulting in dramatically reduced specific energies. One article advocates that lithium overcapacities greater than 100% are unlikely to achieve high cell-level specific energy (4). Several practical studies with specific energies above 300 Wh/kg and

optimized lithium overcapacities optimized for high specific energy support this notion (5-8). Because the failure mechanism of pouch cells tends towards anode degradation rather than polysulfide dissolution, lithium-rich coin cell performance may diminish when adapted into more practical pouch cells with moderate lithium overcapacities (9). To overcome this issue, academia and industry have applied protective coatings to the lithium to prevent degradation via dendrites and parasitic reactions.

Our results show that capacity fade begins to increase in the overcapacity range of 200% and 37% (Figure 11), seemingly consistent with the 100% overcapacity results typically employed in optimized Li-S batteries. It is found that the 3471% and 211% overcapacity results share similar cycle life and starting capacity. Additionally, it seems that a sulfur excess dramatically reduces capacity (Figure 11). Further bracketing of these parameters could reveal a more finely optimized lithium overcapacity. I also recognize that the optimal overcapacity will likely change based on the type of lithium-sulfur battery involved: varying with the amount of parasitic reactions, formation of “dead” lithium, and sulfur utilization.

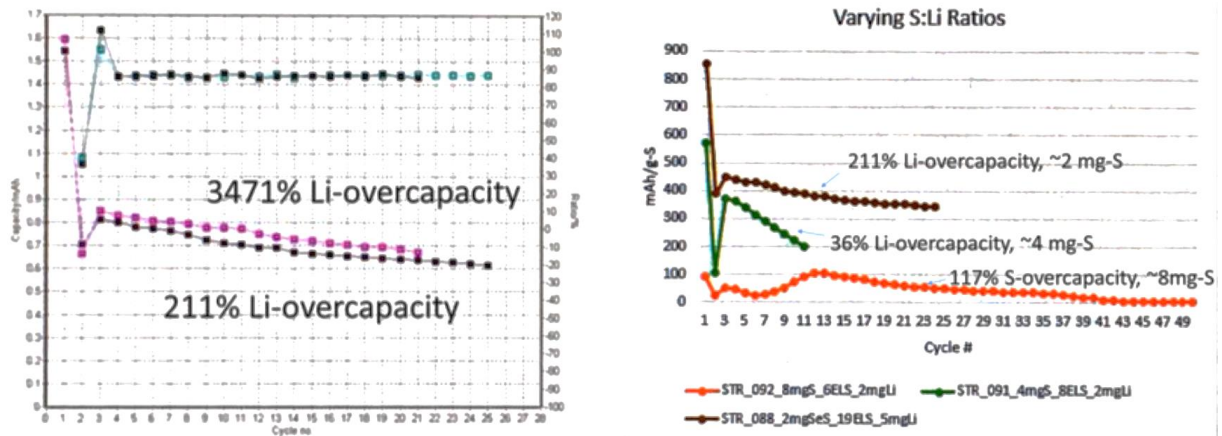


Figure 11. Lithium overcapacity experiments: 3471%, 211%, 36% Li-overcapacity and 117% S-overcapacity shown. 3471% and 211% show similar capacity and cycle life. 36% shows a markedly faster capacity decay. 117% S-overcapacity shows rather poor performance.

3.4 Cycling Conditions

3.4.1 Effect of overcharge end condition

Overcharge cut-off is another method for combatting the low coulombic efficiencies typically associated with lithium-sulfur batteries and the shuttle mechanism. Rather than set a voltage end condition, the battery analyzer can be programmed to stop charging after a certain overcharge has been met. The program analyzes the capacity delivered during the previous discharge and charges the battery to some multiplier of that capacity (e.g. 1.15 corresponding to 15% overcharge). Greater capacity fade is seen with lower overcharges. It does seem however, that cycle life does not begin to significantly decay until somewhere around 15% corresponding to ~87% coulombic efficiency. When micro-patterned CNTs are added, capacity improves even more. Capacity fade, however, does not seem to be significantly affected (Figure 12).

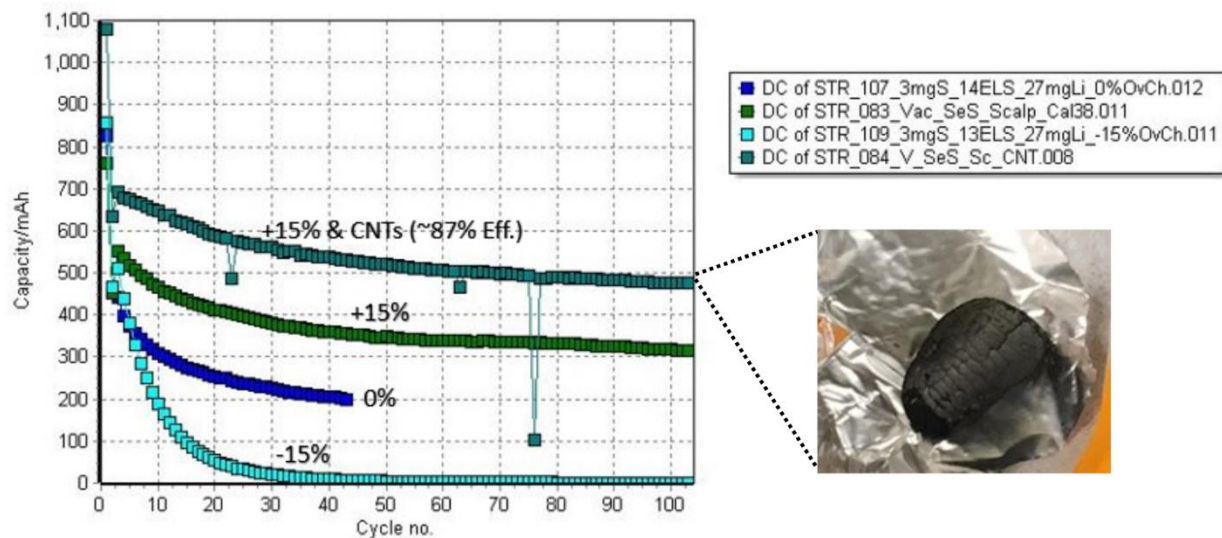


Figure 12. Various overcharge conditions (+15%, 0%, and -15%) are shown, as well as +15% with CNTs added (see image inset). Similar logarithmic trends are seen for each; however, higher overcharge correspond with a better cycle life.

3.5 Slurry Cathode Modifications

Because lithium-sulfur is a potentially low-cost, high-specific energy chemistry, the benefits are mitigated when sulfur comprises only a small portion of the total cathode mass. The active (energy-storing) cathode material mass fraction in lithium-ion batteries typically exceeds 90%. This is possible in part because conductive metals are used as the active material. As discussed earlier, sulfur is a poor conductor, and so a greater percentage of conductive additives (e.g. carbon black) is often used to increase the overall conductivity of the cathode and obtain a better sulfur utilization (closer to its theoretical specific capacity). Doing so introduces trade-offs in performance. Using higher percentages of conductive material and more expensive materials that increase baseline cost may increase sulfur utilization and thereby increase total energy provided per cost (energy affordability). Therefore, any composition will inevitably have certain

mass fractions that optimize energy affordability. Similar logic holds for specific energy as a balance between total energy and total mass is found.

3.5.1 Addition of 1% Se Additive

While use of selenium as a main active material is cost-prohibitive, selenium has been used as an additive in several studies to improve performance in a Li-S battery (10). Because selenium is much more conductive than sulfur, selenium-sulfur composites can form thicker layers when reacted with lithium than stand-alone sulfur counterparts. In this study, 1% selenium replaced 1% of the sulfur, yielding a 1% Se, 69% S cathode composition. While specific capacity did not seem to improve, the battery operated at a higher voltage during discharge (Figure 13). Unexpectedly, at higher C-rates, the capacity (~200 mAh/g at 1 C) did not seem to increase compared with control cells. This suggests that more selenium is needed to significantly affect the conductivity of the cell and thereby active material utilization (specific capacity).

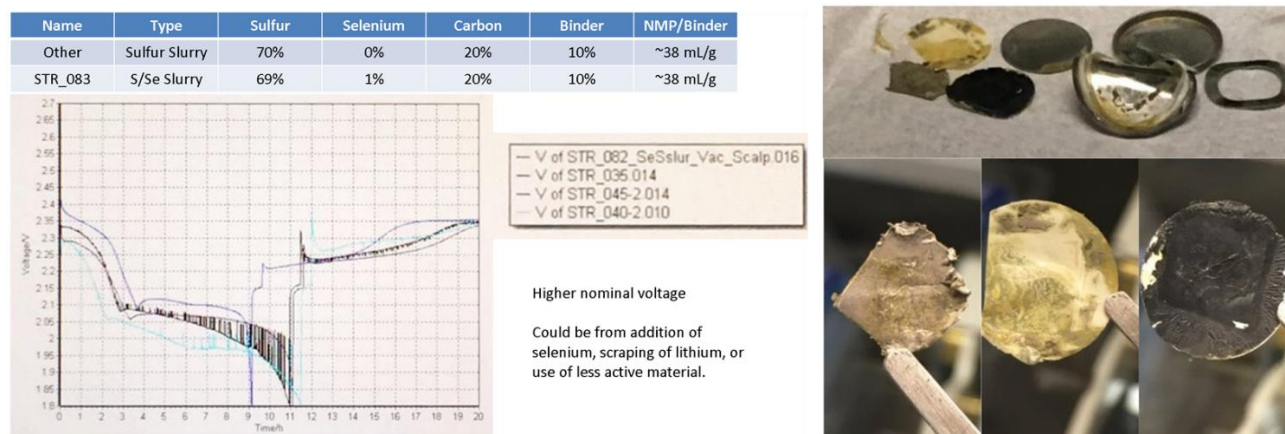


Figure 13. Voltage profiles of Se/S vs. S cathode, first cycle (left) and post-cycled, disassembled high-rate Se/S battery (right).

3.5.2 Addition of PEO/LiTFSI Binder

PEO binder has been shown to help retain polysulfides at the cathode (11). PVdF binder on the other hand is less effective at polysulfide retention. Additionally, PEO/LiTFSI enhances ionic conductivity within the cathode. As such, a PEO/LiTFSI composite was synthesized, mixed with sulfur and CB, and tested in various configurations within the Li-S battery. When a droplet of the composite was dried onto a slurry cathode (total: 4.43 mg-S), cycling results seemed to mimic that of a 2 mg Se/S cathode, and were better than a corresponding 3.88 mg-S cathode. The droplet did not cover the full surface area of the sulfur cathode, and cracks were observed in the structure (Figure 14). The issue of surface coverage could be addressed in a few different ways. More acetonitrile could be added to decrease the viscosity of the compound and thereby induce more surface coverage. A doctor blade could be used to implement the coating. More solution could be added to ensure proper coverage. The issue of cracks would likely be addressed simultaneously with the use of doctor-blade coating before drying the original sulfur cathode. In other words, a dual coating followed by a single drying procedure would likely prevent cracks.

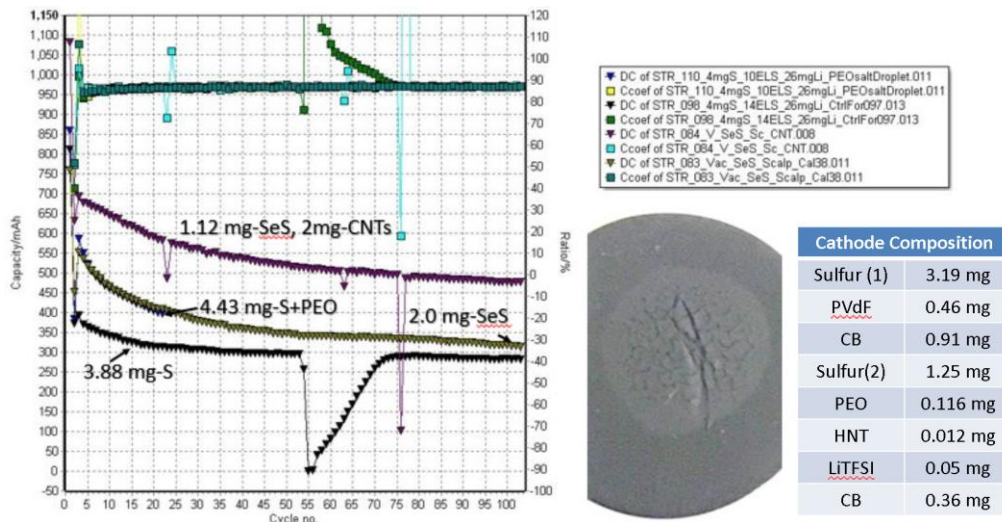


Figure 14. Cycling results of PEO droplet cathode versus other controls.

Two other batteries were assembled and tested. One contained 10.24 mg-S and a micro-patterned CNT interfacial layer. The other contained a small amount of PEO/LiTFSI/S/CB slurry coated onto an aluminum current collector. The high loading sulfur cell exhibited stable cycling, although at a reduced capacity – likely due to a combination of the high sulfur content and correspondingly lower EL:S ratio. The low loading cell similarly exhibited stable cycling, albeit unexpectedly low specific capacity. This could be attributed to either uncertainty in the sulfur mass (via current collector mass or composition uncertainty) or poor conductivity (either electronic or ionic) within the cathode.

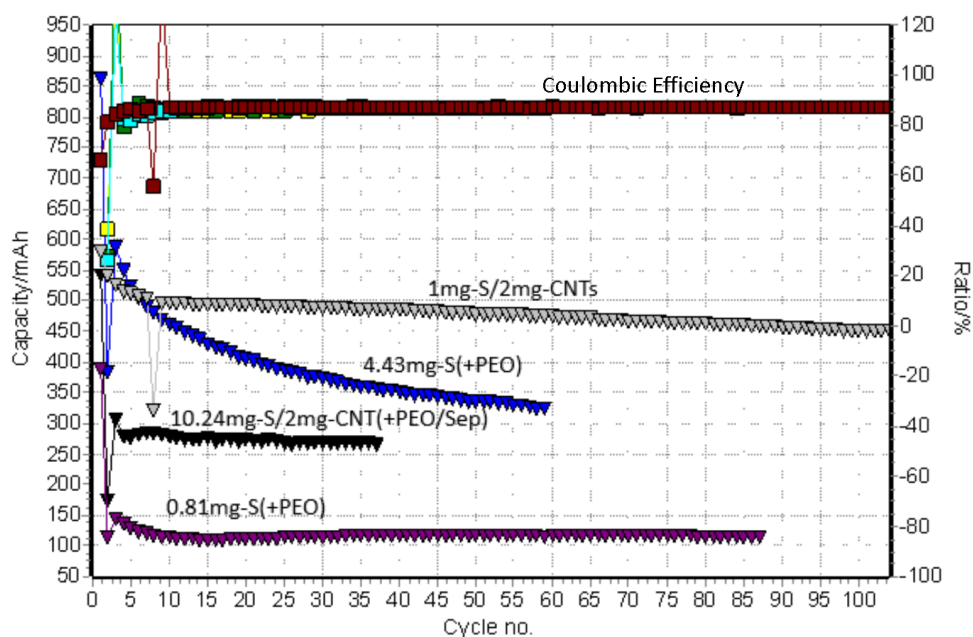


Figure 15. PEO additions.

3.6 Decoupling diffusion and conductivity

It has been unclear to what extent increased capacity and cycle life exhibited by certain CNT-enhanced cells are a result of restricting diffusion via micro-architecture geometries or nanoscale conductivity. An experiment was designed and performed to isolate diffusional effects related to geometry.

First, a sulfur slurry cathode was crimped around a well-intact non-patterned CNT sample, followed by the addition of electrolyte and assembly into a battery (STR_095). Due to a slight break in the cell apparent in the image of STR_095, a small amount of parafilm was stretched onto the crack to prevent diffusion through the gap. During cycling, capacity quickly dropped from $\sim 400 \text{ mAh g}^{-1}$ to $\sim 120 \text{ mAh g}^{-1}$ during the first three cycles. This result suggests that lithium ions may have successfully traversed the encapsulation layer of the CNT architecture; however, performance is worse than stand-alone slurry counterparts. Because the crimping occurred without first adding electrolyte below the CNTs, it's possible that reduced performance correlates with a "dry cathode" rather than slow kinetics of lithium ions across the encapsulation layer. To test this possibility, STR_095 was disassembled, two cuts were made with a scalpel into the CNT architecture, ample electrolyte was added, and the cell was re-assembled (only caps were replaced due to damage during disassembly). By doing so, electrolyte would have greater access to the slurry cathode and lithium-ion diffusion would also be able to occur through the cracks. The discharge capacity of this new cell nearly doubled, as demonstrated by STR_096, though is still low compared to stand-alone slurry cathodes.

Three more cells were assembled using aluminum foil discs. Nine small holes were punched into each of two of the discs using a pronged tool. A slurry cathode was crimped around one of these discs, followed by the addition of electrolyte and cell-assembly (STR_097). Electrolyte was deposited onto a second slurry cathode, followed by placing the other aluminum disc on top, adding more electrolyte, and assembling the cell (STR_099). The last cell – STR_100 – followed a similar procedure to STR_099, but without any holes in the aluminum. As may be expected, STR_099 performs the best at $\sim 85 \text{ mAh g}^{-1}$ owing to the increased presence of electrolyte and lithium access holes. STR_100 delivers $\sim 55 \text{ mAh g}^{-1}$ despite only allowing

lithium access around the edges of the aluminum disc. STR_097 and STR_100 deliver nearly identical capacities at the first discharge, each of which comprise ~65% of the capacity of STR_099 (Figure 16). This suggests that increased electrolyte presence and lithium access both contribute to higher capacity, although the benefit does not seem to be independent of one other (if it were, we would expect the combination of these two capacities to equal the capacity of STR_099).

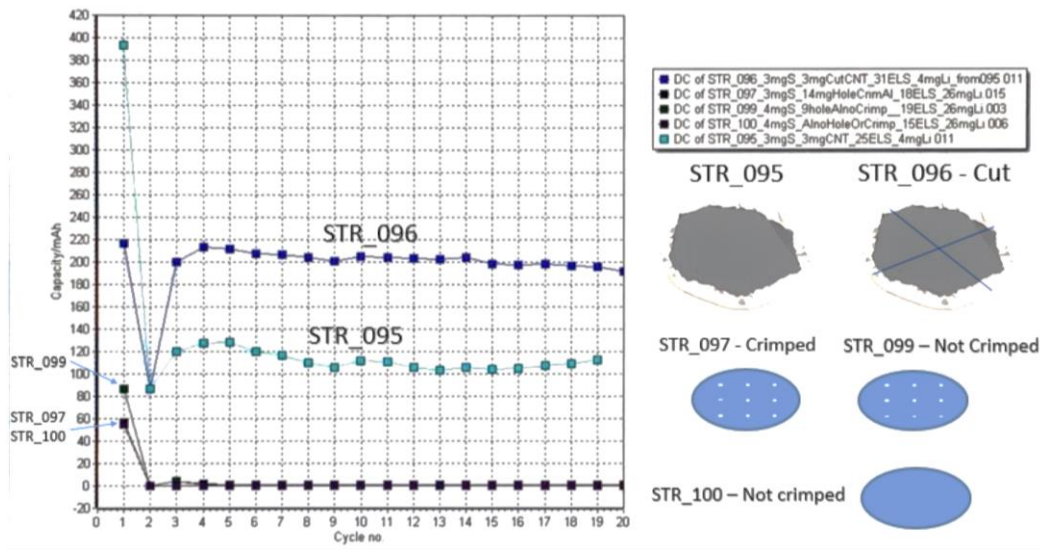


Figure 16. Experiments isolating effects of diffusion and electrolyte presence.

A follow-up experiment that would serve to further isolate the effects of diffusion and conductivity involves obtaining loose MWCNTs with mass and surface area equivalent to the CNT architecture, incorporating them into the cathode slurry, and testing performance. Without an encapsulation layer, diffusion would likely be unaltered while conductivity would be increased.

4 Chapter 4: Conclusions and Future Outlook

4.1 Conclusions

The high coulombic efficiency observed can be attributed to the effectiveness of the carbon-blanket layer in trapping polysulfides and preventing loss of active material/shuttling of sulfur intermediates between anode and cathode. This is indicated by surface morphologies of carbon nanotubes within an interfacial layer post-cycling, as well as by EDS mapping and cycling results. The high sulfur utilization of later cycles likely results from nanoscale contact between sulfur intermediates and the carbon nanotubes, resulting in reutilization of sulfur following dissolution into the electrolyte. Open pore volume—a function of CNT height, diameter, and spacing—must be optimized for an interfacial layer because it can contribute significantly to the overall weight of the battery via necessarily filling it with electrolyte.

To increase cyclability, future work remains in optimizing the thickness of the interfacial layer. This cell design offers a unique architecture for studying ion-transport properties with and without the presence of electrolyte contacting the active material (sulfur).

Alternative methods that mimic such architectures but are optimized for commercial production can be explored to increase affordability and scalability (Figure 17). The sacrificial filling, coating, and filling-removal method used to create thin, low-porosity barriers is particularly noteworthy.

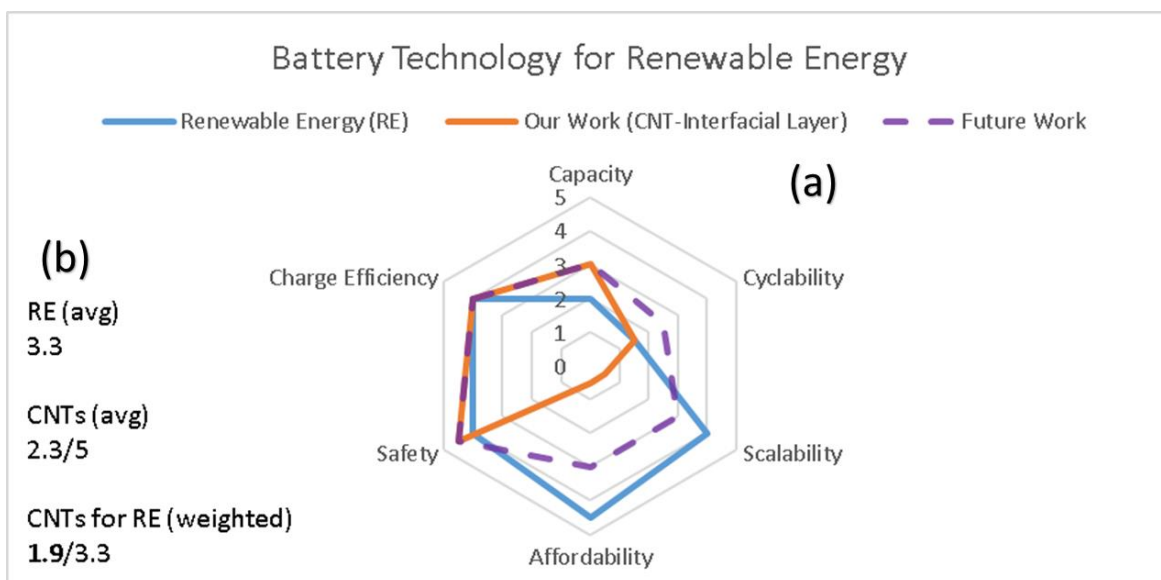


Figure 17. (a) Visual representation (radar chart) of our current carbon nanotube-based lithium-sulfur battery technology compared with renewable energy storage needs and future work. (b) Average scores and weighted averages per specific application-based needs.

Additional studies confirmed that optimal lithium overcapacity for this cell-design occurs between 37% and 200%, in agreement with high-performance Li-S batteries from the literature. An overcharge of 15% was shown to reduce the problems of coulombic inefficiency without greatly sacrificing capacity or cycle life. Small amounts of selenium additive were shown to increase discharge voltage, but without significant gains by way of total energy delivered. Use of PEO-based binders contributed to more stable cycling, but sometimes at lower capacities. Last, enhanced diffusion pathways was shown to increase sulfur utilization independent of electrolytic contact at the cathode.

Thus, a LiNO₃-free, optimized Li-S battery might contain a high-surface area, superficially encapsulated and micro-patterned carbon layer in conjunction with PEO-based slurries, moderate lithium overcapacities, and overcharge rather than voltage end conditions.

4.2 Ideas for enhancing performance

Cycle Life

- Use PEO to reduce polysulfide loss from cathode
- Coating separator with alumina
- Protecting lithium anode with some kind of barrier

Specific Energy

- Use CNT micro-structures to reduce mass of anode and cathode
- **Find optimal EL/S ratio, sulfur load, and S/Li capacity ratio**
- **Assemble small pouch cell or increase CNT size or eliminate wave spring to reduce unnecessary volume and therefore EL**
- Switch to higher SSA carbon to increase specific capacity

Specific Power

- Add 5%+ selenium to increase conductivity
- Increase carbon content in cathode to 30%+
- Increase molarity of EL to 1M+
- Switch to higher SSA carbon

Affordability

- **Restrict NMP amount in cathode slurry**
- Stick with PVdF/Carbon Black/Sulfur slurries
- Find optimal EL/S ratio
- Find optimal EL molarity
- **Reduce area/thickness of lithium metal foil**
- Find optimal S/Li capacity ratio to maximize Li utilization

Safety

- Switch to solid electrolyte or coat separator with alumina or protect lithium anode with barrier to prevent/mitigate dendrites
- Double up on separators to increase separation distance

Storage Characteristics

- Use PEO or CNTs or increase EL molarity or switch to solid electrolyte to reduce PS loss and thereby increase time-energy retention.

Figure 18. Ideas for enhancing performance. Ideas that could potentially increase performance without a trade-off between other metrics are bolded.

5 Appendix A – Supplementary Experiments

5.1 Supplemental Experiment 1

Method:

Make total capacity delivered to the cell (Q_{tot}), discharge current (I_{Dch}), and end conditions ($V_{\text{cut-off}}$, Q_{LHC}) constant for all test conditions (TC#).

Make average charge current ($I_{\text{Avg-Ch}}$) constant for TC1,4:8.

Test condition 1 - slow, continuous charge (e.g. C/10)

Test condition 2 - moderate, continuous charge (e.g. C/2)

Test condition 3 - fast, continuous charge (e.g. 1C)

Test condition 4 - moderate, pulsed charge (e.g. C/2 charge for 1s, rest for 4s)

Test condition 5 - moderate, pulsed charge (e.g. C/2 charge for 2s, rest for 8s)

Test condition 6 - fast, pulsed charge (e.g. 1C charge for 0.5s, rest for 4.5s)

Test condition 7 - fast, pulsed charge (e.g. 1C charge for 1s, rest for 9s)

Test condition 8 - slow, continuous charge (TC1) until 80% of Q_{LHC} , and fast, pulsed charge (TC6) until 115% of Q_{LHC} .

Test condition 9 - slow, continuous charge (TC1) until 80% of Q_{LHC} , and fast, continuous charge (TC3) until 115% of Q_{LHC} .

Predictions:

TC1,4:8 will result in similar capacities (charge and discharge) and coulombic efficiency, with the higher-rate tests exhibiting slightly worse performance. This would indicate that usable charge capacity is primarily a time-dependent process related to diffusion.

Q_{Dch} : TC9 > TC1,4:8 > TC2 > TC3 indicating a trade-off between improving cathode kinetics and reducing self-discharge due to shuttle.

CE: TC3 > TC9 > TC2 > TC1,4:8 indicating that time for the shuttle effect to occur is restricted.

5.2 Supplemental Experiment 2

Method:

Place lithium metal and sulfur into an electrolyte solution (LiTSFI in DME/DIOX) to generate polysulfides. (*Determine the change in mass of the cathode, the lithium, and the electrolyte solution.*)

Place a new sulfur cathode into the solution and let stand for 5 minutes. Rinse in a blank DME solution and let soak in a separate one for 5 minutes and let it dry. Note the change in mass of the first solution, the mass added to the blank solution, and the change in mass of the sulfur cathode.

Prediction:

There will be a net mass added to the two solutions resulting from the dissolution of polysulfides from the new cathode into the two solutions.

If there is no net mass change, or there is a net mass loss from the two solutions, this could indicate that a significant chain reaction did not occur. This would still be consistent with the proposed mechanism of a balancing reaction during charge.

Controls:

Sandwich Li and S-cathode and place into blank EL solution (DME/DIOX only, no LiTSFI)

Place S-cathode into blank EL solution, remove, and let dry. Determine change in mass.

Place S-cathode into EL solution, remove, and let dry. Determine change in mass.

Place just alligator clips into the EL solution, remove, and determine the mass change of the electrolyte over some amount of time (change in mass due to evaporation and removal of clips)

Place just alligator clips into blank EL solution, remove, and determine the mass change of the electrolyte over some amount of time (change in mass due to evaporation and removal of clips)

Repeat the procedure under "Method" except without the rinse in a blank DME solution.

6 Appendix B – Challenges of the Lithium-Sulfur Chemistry

Some information here is repeated in the previous main-body sections but is provided again in a single location for convenience of the reader.

6.1 Physical challenges of the lithium-sulfur chemistry

6.1.1 Conductivity of sulfur

Sulfur is a very poor conductor, meaning it has a high resistivity ($\sim 1 \times 10^{15} \text{ m } \Omega$). This necessitates the use of conductive additives (e.g. carbon black) to compensate and increase the overall conductivity of the cathode.

6.1.2 Volume expansion of sulfur

When fully converted from elemental sulfur to lithium sulfide, the compound undergoes a volume expansion of $\sim 80\%$, potentially causing mechanical fracture and loss of reaction sites. The problem is accentuated at deeper discharges and when active material is better retained at the cathode (see dissolution of polysulfides). Researchers have employed various 1D, 2D, 3D, and hierarchically structured cathode designs that can help mitigate this issue (12-15).

6.1.3 Dissolution of polysulfides

Once elemental sulfur is converted into intermediate lithium “polysulfides,” the active material becomes soluble in organic electrolytes (except for the final state of lithium sulfide) and is free to diffuse throughout the battery unless otherwise restricted.

6.1.4 Lithium dendrites

Lithium dendrites are a common plague for any lithium-based battery; however, the problem is often worse when pure lithium-metal is used as the anode. Non-uniform electric fields and other local stresses can lead to lithium plating in the form of dendrites that can either reduce usable lithium capacity or cause a potentially dangerous internal short-circuit.

6.1.5 Parasitic reactions of polysulfides with electrolyte/anode

The diffusion of polysulfides onto the anode surface has been shown to reduce lithium dendrite formation; however, parasitic reactions also can occur together with the electrolyte and/or the anode, further reducing the usable sulfur amount and increasing internal resistance in the battery.

6.1.6 Polysulfide shuttle mechanism

Not only can polysulfides be lost from the cathode and detrimentally reacted at the anode, they can also be reduced to a state closer to lithium-sulfide (fully-discharged) during the charge procedure and proceed to diffuse back towards the cathode. There they can be converted again to a state closer to elemental sulfur (fully-charged) and will travel back to the anode to repeat the process. This process known as “shuttle” leads to low coulombic (charge) efficiency and even an “infinite charge syndrome” in some cases.

6.2 Practical challenges of commercializing lithium-sulfur batteries

6.2.1 Cathode mass fraction

Because lithium-sulfur is a potentially low-cost, high-specific energy chemistry, the benefits are mitigated when sulfur comprises only a small portion of the total cathode mass. The active (energy-storing) cathode material mass fraction in lithium-ion batteries typically exceeds 90%. This is possible in part because conductive metals are used as the active material. As discussed earlier, sulfur is a poor conductor, and so a greater percentage of conductive additives (e.g.

carbon black) is often used to increase the overall conductivity of the cathode and obtain a better sulfur utilization (closer to its theoretical specific capacity). Doing so introduces trade-offs in performance. Using higher percentages of conductive material and more expensive materials that increase baseline cost may increase sulfur utilization and thereby increase total energy provided per cost (energy affordability). Therefore, any composition will inevitably have certain mass fractions that optimize energy affordability. Similar logic holds for specific energy as a balance between total energy and total mass is found.

6.2.2 Sulfur loading

High sulfur loading can increase energy affordability and specific energy by increasing the fraction of sulfur compared with other inactive components such as current collectors, separators, and battery housing. As sulfur load increases, electronic and ionic resistance can begin to dominate as transport lengths increase and reaction sites are shielded. This leads to reduced sulfur utilization, suggesting an optimal sulfur load for best performance.

6.2.3 Electrolyte to Sulfur Ratios

Lithium-sulfur batteries tend to require much higher electrolyte to active mass ratios (e.g. > 5:1) than traditional lithium-ion batteries (~1:1). When electrolyte to sulfur (EL:S) ratios are too low (e.g. < 5:1), increased electrolyte viscosity will dramatically increase cell resistance and thereby lower sulfur utilization in many Li-S configurations (*1*). When EL:S ratios are exorbitantly high (e.g. > 15:1), the advantage of high theoretical specific energy is forfeited. Additionally, because this metric affects performance through electrolyte viscosity and cell impedance, the performance of electrolyte-flooded coin cells will not necessarily correlate with the performance of electrolyte-lean pouch cells.

6.2.4 Lithium overcapacity

Lithium overcapacity refers to the excess stoichiometric amount of lithium compared with the sulfur active material present in the battery. A lithium overcapacity of 0% means that for complete conversion of all elemental sulfur and lithium into lithium-sulfide, all reactants will be used up. It is recognized that some excess amount of lithium is necessary for the proper functioning of lithium-sulfur and other lithium-metal chemistries (2-4). In many studies, lithium overcapacity exceeds 3000%, resulting in dramatically reduced specific energies. One article advocates that lithium overcapacities greater than 100% are unlikely to achieve high cell-level specific energy (4). Several practical studies with specific energies above 300 Wh/kg and optimized lithium overcapacities optimized for high specific energy support this notion (5-8). Because the failure mechanism of pouch cells tends towards anode degradation rather than polysulfide dissolution, lithium-rich coin cell performance may diminish when adapted into more practical pouch cells with moderate lithium overcapacities (9). To overcome this issue, academia and industry have applied protective coatings to the lithium to prevent degradation via dendrites and parasitic reactions.

6.2.5 Low coulombic efficiency/infinite-charge syndrome

Low coulombic (charge) efficiency results from the “shuttle” effect occurring in lithium-sulfur batteries. During charge, polysulfides that diffuse towards the anode can be reduced to a lower charge state, shuttle back to the cathode, and repeat the process. Both engineering and administrative strategies have been employed to overcome this issue. The containment or “trapping” of polysulfides within the cathode is a focus of many research investigations. Other strategies focus on passivating or insulating the lithium anode, thereby preventing unwanted polysulfide reduction from occurring. Lithium-nitrate is often used as an additive to create a

stable solid electrolyte interphase (SEI) layer but is impractical due to safety issues. A less common strategy involves setting an upper limit on the overcharge compared with the capacity delivered during the previous cycle. For example, 15% overcharge means that the battery will charge 115% of the previous half-cycle, resulting in ~87% coulombic efficiency. Despite never reaching the cut-off voltage, the battery can still achieve good cycle life.

6.2.6 Low cycle life

The continuous loss of sulfur through dissolution out of the cathode and parasitic reactions combined with sustained anode degradation and decreased reaction sites via volume expansion result in low cycle life. These issues can be addressed through sulfur “trapping” mechanisms, anode protection, robust architectures, and optimized pore volumes, among other methods.

7 Appendix C – Chain reaction effects

During one experiment, a freshly assembled lithium-sulfur battery was first charged and immediately rose from ~2.4 V to 2.6 V meeting the upper voltage cut-off limit. Next, the battery underwent a slight discharge at 0.05 C for ~10 seconds delivering # mAh of capacity. The battery then charged for several minutes at the same 0.05 C-rate, followed by a few minutes of charging at 1C before reaching 2.6 V. The charge and discharge capacities varied by several orders of magnitude, indicating a possible chain reaction moving the battery from a stable to instable state. Approximately 3 mg of sulfur was contained within the battery. Assuming a mild conversion from elemental S₈ sulfur to Li₂S₆ (full conversion being until Li₂S), #% of the sulfur would have been affected by this discharge. The large overcharge supplied to the battery while at 0.05 C could be explained by the shuttle effect and corresponding low efficiencies; however, when Li-S batteries are charged at rates as high as 1C, the shuttle mechanism is unlikely to

dominate as supported by the corresponding high coulombic efficiencies (>90%) associated with high-rate cells.

It seems clear that some chain reaction occurs, but explaining what is happening and why becomes a more difficult challenge. It is known that lithium-sulfur batteries exhibit higher self-discharge when stored at higher states of charge (*RW.ERROR - Unable to find reference:doc:5b6681a1e4b07290536028d9*), and that self-discharge has been linked to the polysulfide shuttle mechanism (16); yet, the 1C charging seems to contradict that link. The contradiction could be explained by polysulfide “seeds” leading to further breakdown of elemental sulfur within the cell. Such a mechanism would require a supply of electrons to facilitate the conversion as explained. First, a slight discharge generates high order polysulfides (HPS) that diffuse to the lithium. Second, during a slow charge, HPS reduce to low order polysulfides (LPS) and diffuse back to the cathode consistent with the shuttle mechanism. Third, LPS balance with elemental sulfur at the cathode to form HPS, leading to progressively higher amounts of polysulfide as charge continues. Eventually, this could lead to all elemental sulfur being converted to polysulfides despite having undergone minimal discharge. Thus, charge conservation still holds via electrons supplied during charge, and the orders of magnitude difference between fast charge and slow discharge are explained by a combination of shuttling and balancing reactions during slow charge. A simple experiment could be designed with short duration, low discharge followed immediately by long duration, high charge to quantify the time dependence (and hence diffusion characteristics) of this system.

Additional unperformed experiments outlined in Appendix A – Supplementary Experiments could further verify or disprove this hypothesis.

7.1 CNT Parameters

7.1.1 Un-patterned, encapsulated CNTs

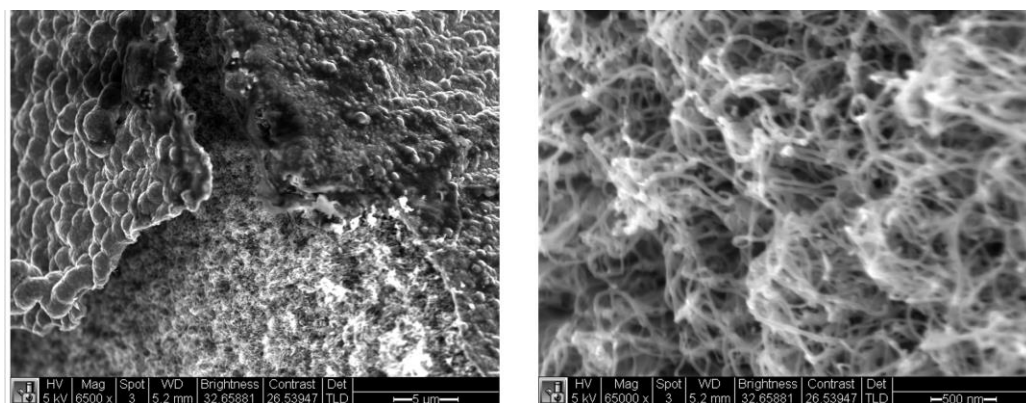


Figure 19. Encapsulated, un-patterned sample from top-view at 45° tilt.

7.1.2 Presence of floor layer in encapsulated cells

Varying CNT parameters allowed for the inclusion or exclusion of a floor layer associated with the substrate facing side of the CNT structure. This property is important because it affects both lithium-ion and polysulfide diffusion within the battery.

CNTs fabricated with 585°C LPCVD Si-infiltration and a 20-minute carbon encapsulation yielded no holes in the floor layer. Meanwhile, CNTs fabricated with a 535°C Si-infiltration and a 30-minute carbon encapsulation yielded holes in the floor layer (Figure 20). While one might expect no holes after longer carbon encapsulation, it seems that shorter carbon infiltration time and higher LPCVD temperature resulted in holes. However, it is possible that a shorter infiltration time yielded a less robust encapsulation layer and less internal stress such that the floor layer adhered better to the substrate. In this case, the inside pillars may have detached from the underlying floor layer which seems most consistent with pillar edge morphologies as observed by SEM (Figure 20). It is also possible that the higher LPCVD temperature led to less uniform surface morphology and therefore higher surface area, further increasing the adherence

of the carbon to what was beneath. Whatever the underlying mechanism, it seems quite clear and repeatable that these difference in parameters caused either the presence or lack of a floor layer as stated.

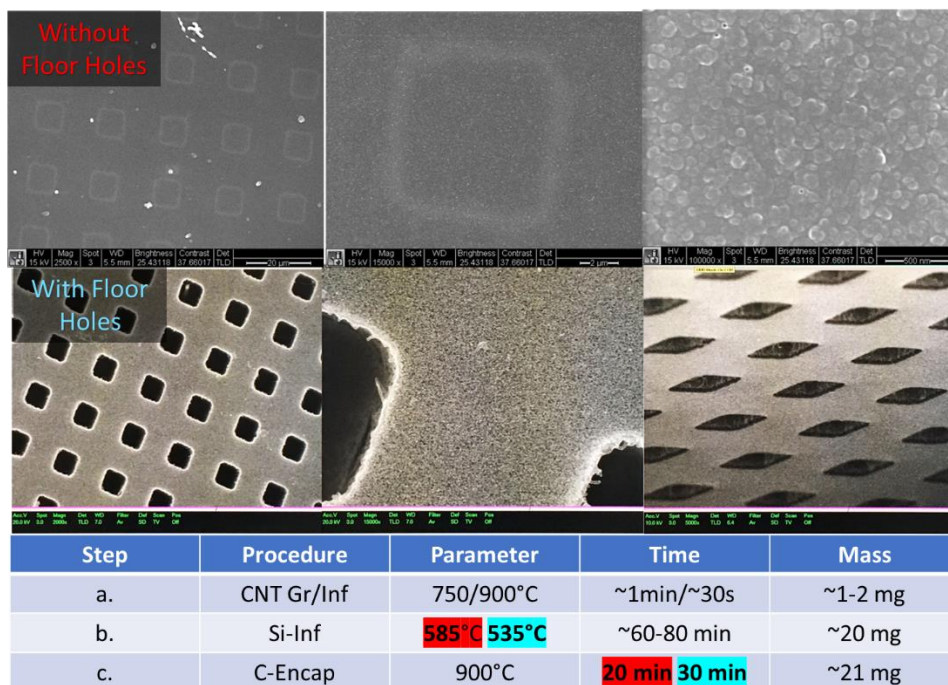


Figure 20. CNTs with versus without holes in floor layer and corresponding parameters.

Parameters adjusted to for no floor layer highlighted in red.

Which of these are more favorable for fabrication of the cell depends to a large extent on the underlying mechanisms of lithium-ion transport and characteristics of the polysulfide diffusion within the battery. If lithium—whether in the form of an ion or as metallic lithium—can transport across the thin carbon encapsulation layer (~100 nm) as the dominant transport mechanism, then including a floor layer to completely retain polysulfides within the cathode is the most favorable option. On the other hand, if lithium cannot kinetically transport across the carbon barrier (instead being restricted to diffusion through open channels), then excluding the floor layer to promote lithium-ion accessibility makes more sense. In this case, the geometry of

the micro-structure must be optimized to allow lithium-ion diffusion to occur while still restricting polysulfide diffusion. Based on previous results, it appears that small, well-spaced fissures allow for higher rate capabilities and better capacity retention, consistent with open channel diffusion as the dominant mechanism. Numerical modeling may prove useful in assessing optimal geometries that balance this trade-off between lithium-ion and polysulfide diffusion.

8 Appendix D – Supplementary Experimental Methods

8.1 SEM and EDS characterization of samples

One of the issues of SEM characterization with fragile samples such as the CNT structures is that samples used for ex-situ characterization could not easily be used for electrochemical. Thus, a method was developed that allows the CNT layer to remain intact and later be used in a battery.

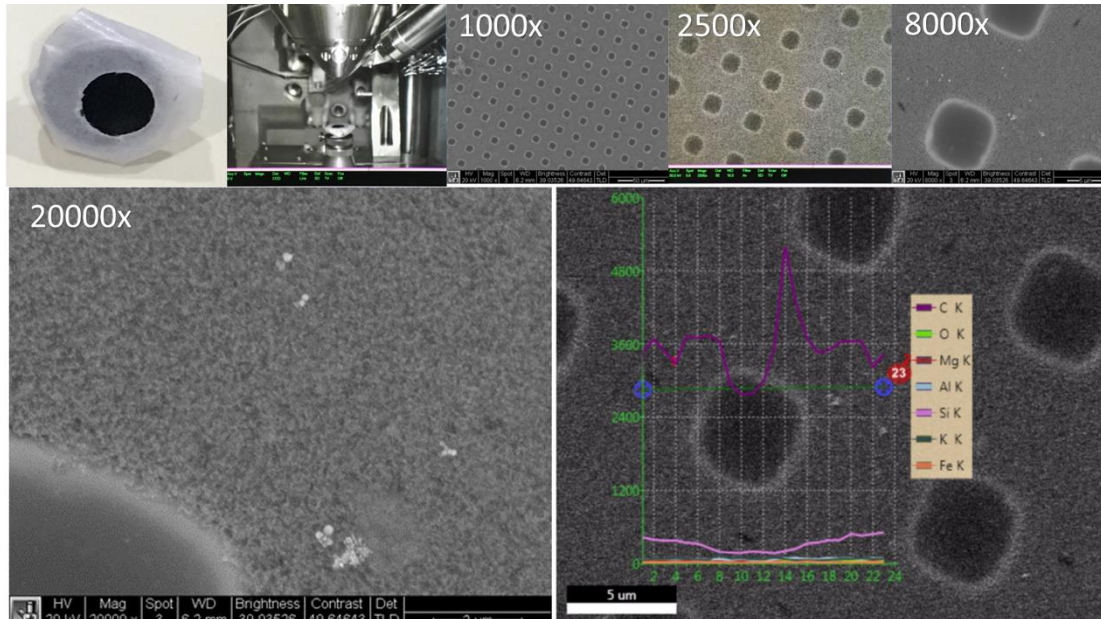


Figure 21. A method for non-destructive SEM was developed by wrapping a piece of weigh paper around the CNT layer situated on top of an aluminum SEM stub (top-left). Various SEM images and EDS data were obtained using this method.

8.1.1 Calendaring

Preliminary results suggest that calendaring the cathodes may have had a positive impact.

However, differences were within reasonable uncertainties, necessitating further repeats to confirm the positive effects of calendaring.

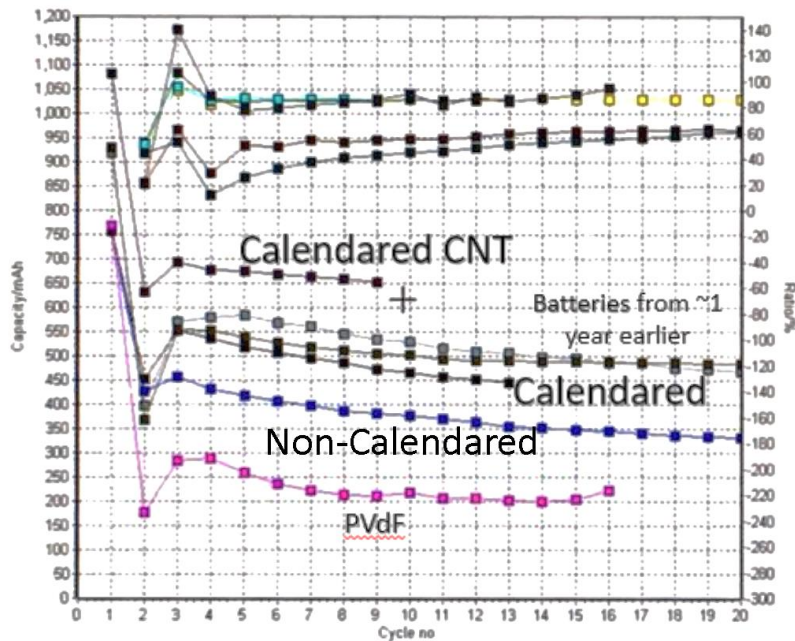


Figure 22. Calendared electrodes vs. non-calendared electrodes.

8.2 Roll Press Modifications (2018-06w1,2...pptx on box)

8.2.1 Free-standing slurry electrodes via roll-press

A new method was developed to create free-standing slurry electrodes. A large area free-standing slurry was made (~4 cm x 3 cm). When using the roll-press to coat slurry onto Celgard separator material, both sides needed to be coated for the separator to not curl up. Several practical options exist to prevent significant curling. First, a thick coating could be applied to one side with a thinner coating applied to the other. Second, a relatively thin coating could be applied to one side of the separator to reduce the stresses involved. Third, a thin piece of lithium could be

attached at the other side to provide better structural support (2.4). The cycling results of such free-standing cathodes have not been tested.

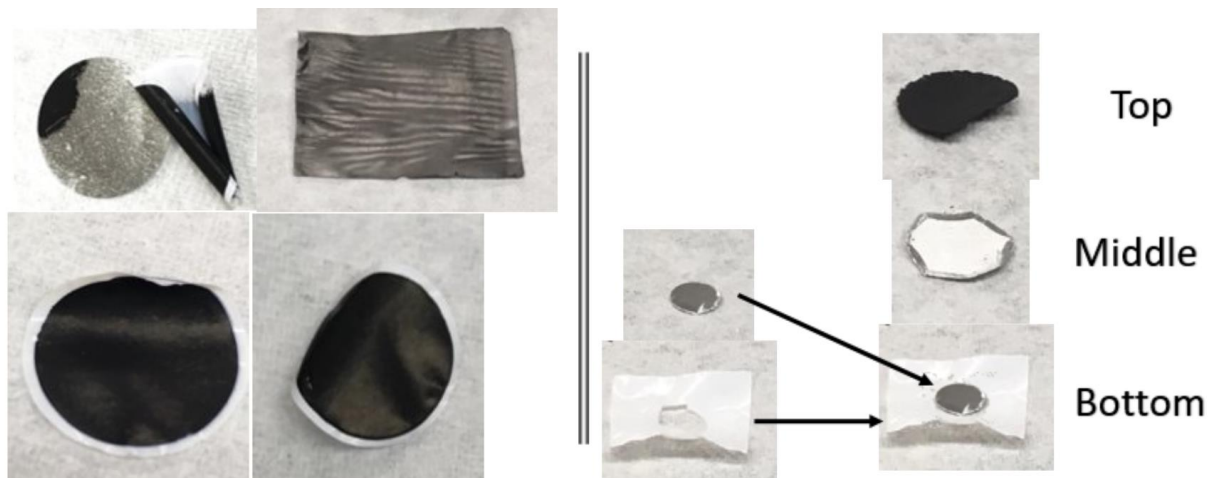


Figure 23. Various options for roll-press modification (left) and concept experiment (right).

I also found that thinner slurry cathodes (less than 1.5 mg-S/cm²) exhibited regular calendaring behavior when roll-pressed without IPA. A medium range of slurry cathodes (1.5 mg-S/cm² to 2.5 mg-S/cm²) exhibited imperfect delamination into a free-standing electrode. Larger slurry cathodes (greater than 2.5 mg-S/cm²) tended to readily delaminate into free-standing cathodes.

8.2.2 Roll-press of CNTs and cathode slurry

When micro-patterned CNTs were roll-pressed against a sulfur slurry cathode, the slurry delaminated from the aluminum foil and adhered to the CNTs. It was found that when a mesh-patterned CNT structure was used as the “upper current collector,” the composite structure developed many fissures. When an un-patterned structure was used, very few fissures developed. Despite having many fissures, the modified patterned-CNT/sulfur-slurry cathode remained intact upon assembly and delivered the best cycling/capacity results obtained out of ~100 batteries assembled to date.



Figure 24. Pressing CNTs and a sulfur slurry (~0.05 mm) resulted in a delaminated slurry and cracked CNTs (bottom-left). The leftover slurry and aluminum foil are shown in the (top-middle).

The weight reduction of ~10 mg by utilizing the CNT structures as an upper current collector is a further benefit. This would allow for a weight reduction of ~20% in an optimized configuration (e.g. 3-5 mg-S/cm², 5 EL:S, 100% Li-overcapacity).

8.3 Lithium anode modifications

8.3.1 Lithium melt infiltration into CNTs via LPCVD lithophilic coating

A lithium melt infiltration similar to that reported by ... was implemented with a CNT forest. A light coating of silicon was deposited via LPCVD followed by a lithium melt in an argon glovebox using a hotplate. The lithium melt was somewhat unsuccessful – the CNTs were ripped apart in the middle by what appears to have been surface tension due to cooling. Additionally, the CNTs and lithium were heated past the melting point of lithium, resulting in burned lithium. It was later discovered that due to the high melting point of oxide layers that form on lithium metal, the lithium foil should have first been scraped off with a scalpel.

Type	Growth/Inf	Height	CNT Mass	Si Mass	Li Mass	Total Mass	Porosity
Anode	60min/2min	~600 um	3.31 mg	0.35 mg	11.6 mg	--	~53%



Figure 25. Somewhat unsuccessful lithium melt infiltration into CNT forest. Various parameters associated with the experiment (top), Pre-LPCVD forest (left), molten lithium and oxides atop Si-coated forest (middle) and burned lithium atop cracked CNTs due to high temperature (right).

It is also possible that even with a successful melt infiltration, re-deposition of lithium onto the surface rather than within the CNT microstructure (i.e. on the walls of the CNTs) may be more energetically favorable. This would mitigate the benefits of a lithium-melt procedure after the first cycle. Due to these issues, an alternative method using roll-press is preferred (Figure 26).



Figure 26. Small piece of oxide-removed lithium metal foil sitting atop Celgard inside a hydraulic press (left). Lithium metal after sandwiching between two pieces of Celgard, pressing via hydraulic press, and peeling off one of the Celgard layers.

8.4 Bibliography

- (1) Chen, S.; Yu, Z.; Gordin, M. L.; Yi, R.; Song, J.; Wang, D. A Fluorinated Ether Electrolyte Enabled High Performance Prelithiated Graphite/Sulfur Batteries. *Acs Applied Materials & Interfaces* **2017**, *9*, 6959-6966, DOI: 10.1021/acsami.6b11008.
- (2) Hagen, M.; Fanz, P.; Tübke, J. Cell energy density and electrolyte/sulfur ratio in Li-S cells. *Journal of Power Sources* **2014**, *264*, 30-34, DOI: 10.1016/j.jpowsour.2014.04.018.
- (3) Eroglu, D.; Zavadil, K. R.; Gallagher, K. G. Critical Link between Materials Chemistry and Cell-Level Design for High Energy Density and Low Cost Lithium-Sulfur Transportation Battery. *Journal of The Electrochemical Society* **2015**, *162*, A990, DOI: 10.1149/2.0611506jes.
- (4) Brueckner, J.; Thieme, S.; Grossmann, H. T.; Doerfler, S.; Althues, H.; Kaskel, S. Lithium-sulfur batteries: Influence of C-rate, amount of electrolyte and sulfur loading on cycle performance. *J. Power Sources* **2014**, *268*, 82-87, DOI: 10.1016/j.jpowsour.2014.05.143.
- (5) Ma, Y.; Zhang, H.; Wu, B.; Wang, M.; Li, X.; Zhang, H. Lithium Sulfur Primary Battery with Super High Energy Density: Based on the Cauliflower-like Structured C/S Cathode. *Scientific reports* **2015**, *5*, 14949, DOI: 10.1038/srep14949.
- (6) Liu, Z.; Zheng, X.; Yuan, N.; Ding, J. A novel device structure for a low-cost Li-S battery. *Journal of Materials Chemistry a* **2017**, *5*, 942-946, DOI: 10.1039/c6ta08828g.
- (7) Zhang, J.; Wang, D.; Xu, W.; Xiao, J.; Williford, R. E. Ambient operation of Li/Air batteries. *Journal of Power Sources* **2010**, *195*, 4332-4337, DOI: 10.1016/j.jpowsour.2010.01.022.
- (8) Wang, L.; He, X.; Li, J.; Gao, J.; Fang, M.; Tian, G.; Wang, J.; Fan, S. Graphene-coated plastic film as current collector for lithium/sulfur batteries. *Journal of Power Sources* **2013**, *239*, 623-627, DOI: 10.1016/j.jpowsour.2013.02.008.

- (9) Cheng, X.; Yan, C.; Huang, J.; Li, P.; Zhu, L.; Zhao, L.; Zhang, Y.; Zhu, W.; Yang, S.; Zhang, Q. The gap between long lifespan Li-S coin and pouch cells: The importance of lithium metal anode protection. *Energy Storage Materials* **2017**, *6*, 18-25, DOI: 10.1016/j.ensm.2016.09.003.
- (10) Li, X.; Liang, J.; Zhang, K.; Hou, Z.; Zhang, W.; Zhu, Y.; Qian, Y. Amorphous S-rich S_{sub(1-x)}Se_{sub(x)}/C (x less than or equal to 0.1) composites promise better lithium-sulfur batteries in a carbonate-based electrolyte. *Energy & Environmental Science* **2015**, *8*, 3181-3186, DOI: 10.1039/c5ee01470k.
- (11) Bresser, D.; Passerini, S.; Scrosati, B. Recent progress and remaining challenges in sulfur-based lithium secondary batteries - a review. *Chem. Commun.* **2013**, *49*, 10545-10562, DOI: 10.1039/C3CC46131A.
- (12) Dorfler, S.; Hagen, M.; Althues, H.; Tubke, J.; Kaskel, S.; Hoffmann, M. J. High capacity vertical aligned carbon nanotube/sulfur composite cathodes for lithium-sulfur batteries. *Chem. Commun.* **2012**, *48*, 4097-4099, DOI: 10.1039/C2CC17925C.
- (13) Zhang, Y.; Yan, Y.; Xie, J.; Cui, N.; Pan, Z.; Hao, C. Ionothermal synthesis of graphene-based microporous carbon for lithium-sulfur batteries. *New Journal of Chemistry* **2018**, *42*, 2483-2490, DOI: 10.1039/c7nj04294a.
- (14) Li, F.; Zhao, J. Three dimensional porous SiC for lithium polysulfide trapping. *Physical Chemistry Chemical Physics* **2018**, *20*, 4005-4011, DOI: 10.1039/c7cp07113b.
- (15) Zhao, Y.; Tan, R.; Yang, J.; Wang, K.; Gao, R.; Liu, D.; Liu, Y.; Yang, J.; Pan, F. 3D-hybrid material design with electron/lithium-ion dual-conductivity for high-performance Li-sulfur batteries. *Journal of Power Sources* **2017**, *340*, 160-166, DOI: 10.1016/j.jpowsour.2016.11.067.

(16) Mikhaylik, Y. V.; Akridge, J. R. Polysulfide Shuttle Study in the Li/S Battery System. *J. Electrochem. Soc.* **2004**, *151*, A1976, DOI: 10.1149/1.1806394.

8.5 Index

- Cathode Composition..... 6, 37
CNT.... 1, 2, 6, 10, 12, 15, 16, 18, 19, 26, 27, 29, 30, 41, 42, 44, 46, 47, 48
Conductivity. 5, 9, 10, 23, 24, 25, 26, 27, 29, 35, 37, 51
Cost 7, 8, 9, 23, 24, 37, 49, 50
Coulombic Efficiency 6, 9, 15, 18, 22, 29, 33, 39
Cycle Life. 2, 6, 9, 14, 18, 21, 22, 23, 24, 27, 31, 39, 48, 50
Dendrites 5, 8, 21, 36, 39
Diffusion 6, 34, 40
Electrolyte to Sulfur Ratio . 5, 10, 19, 20, 26, 38, 47
Encapsulation Layer... 15, 16, 18, 19, 27, 29, 42, 43
Free-Standing Electrodes 6, 45, 46
Interfacial Layer. 2, 5, 10, 11, 12, 13, 16, 18, 26, 29, 30
 Thickness..... 30
LiNO₃ 1, 2, 9, 10, 15, 16, 31
Lithium Overcapacity 2, 5, 10, 14, 20, 21, 31, 38
Micro-patterning 3, 10, 15, 22, 26, 27, 29, 30, 31, 46
Optimization 24, 37
Overcharge.... 2, 5, 10, 22, 23, 31, 32, 39, 40
PEO 2, 5, 25, 26, 27, 31, 32
polysulfide..... 21, 25, 38, 39, 40, 42, 43, 51
Polysulfide ... 2, 6, 21, 25, 36, 38, 39, 40, 42, 43, 51
Roll-Press..... 6, 45, 46, 48
Safety 1, 2, 9, 10, 15, 16, 31
Selenium Additive 2, 19, 24, 31
SEM 5, 6, 14, 16, 17, 42, 44
Shuttle Mechanism... 6, 8, 18, 22, 34, 36, 39, 40, 51
Slurry 5, 6, 10, 11, 17, 18, 23, 25, 26, 27, 28, 29, 45, 46, 47
Specific Capacity 7, 20, 23, 24, 26, 37
Specific Energy 1, 2, 7, 19, 20, 21, 23, 37, 38
Sulfur Load 2, 5, 6, 10, 15, 19, 20, 37, 49
Volume Expansion..... 5, 8, 9, 10, 35, 39